This is the accepted manuscript (postprint) of the following article:
E. Salahinejad, R. Vahedifard, *Deposition of nanodiopside coatings on metallic biomaterials to stimulate apatite-forming ability*, Materials and Design 123 (2017) 120–127.
http://dx.doi.org/10.1016/j.matdes.2017.03.047

Deposition of nanodiopside coatings on metallic biomaterials to stimulate apatite-forming ability

Erfan Salahinejad *, Reza Vahedifard

Faculty of Materials Science and Engineering, K.N. Toosi University of Technology, Tehran, Iran

Abstract

One of the drawbacks of metals and alloys in biomedical applications is their inefficient fixation to adjacent tissues which can be fairly addressed by applying bioactive ceramic coatings. In this work, colloidal suspensions based on coprecipitation-derived nanoparticulate diopside ($CaMgSi_2O_6$) were deposited on stainless steel 316L by dip-coating and subsequent low-temperature sintering. Afterwards, the structure, bioactivity and biodegradation of the samples were *in vitro* evaluated by spectroscopic and microscopic techniques. The apatite-forming ability of the surface was found to be improved by using the nanodiopside coating, while controlled by a typical ion-exchange reaction mechanism originating from the film's degradability. In this regard, after soaking the coated samples in a simulated body fluid, an integrated leaf-like precipitation of apatite at early stages and a following non-uniform rose-like growth of apatite with an increased level of the carbonate substitution for hydroxyl were detected. It is eventually concluded that nanodiopside coatings deserve further consideration and development in the biomedical field, where a bioactive fixation is needed along the implant/tissue interface.

* Corresponding Author: Email Addresses: <salahinejad@kntu.ac.ir>, <erfan.salahinejad@gmail.com>

This is the accepted manuscript (postprint) of the following article:
E. Salahinejad, R. Vahedifard, *Deposition of nanodiopside coatings on metallic biomaterials to stimulate apatite-forming ability*, Materials and Design 123 (2017) 120–127.
http://dx.doi.org/10.1016/j.matdes.2017.03.047

Keywords: Diopside; Coating; Bioactivity; Biodegradation

1. Introduction

Metals and alloys are widely used in the different fields of biomedicine, such as orthopedic, dental, cardiovascular and hyperthermia applications [1-4]. The main advantage of this classic group of biomaterials is that they offer a desirable combination of mechanical strength and toughness. On the other hand, they suffer from a number of drawbacks like corrosion and inefficient bioactivity. The former can result in an early fracture failure and/or the detrimental influence on biocompatibility. Also, because of the latter limitation, the metallic biomaterial is deprived of a desirable fixation to neighboring tissues, which can lead to the implant's loosening, feeling pain and/or mechanical damage to adjacent tissues [5, 6]. These surface-relating disadvantages can be fairly overcome by applying coatings on the metallic implants [7-17].

Among the various types of biomaterials, a number of ceramics present the most bioactivity via the formation of an apatite layer on their active surface, leading to a chemical bonding to adjacent tissues. Typical examples for these bioceramics include bioactive glasses, glass-ceramics and calcium phosphates. A newer family of ceramics, belonging to the SiO_2-CaO-MgO system, is currently under consideration, due to its superior fracture toughness and osteoinductivity [18, 19]. One of the members of this system is diopside ($MgCaSi_2O_6$) with a monoclinic pyroxene structure and a melting point of 1391 °C. In regard to bioactivity, diopside is degraded and substituted by new bone with a relatively desired speed, while the rest yields a homogeneous bonding to newly-grown bone [18, 20].

In general, the use of wet-chemical synthesis techniques like coprecipitation and sol-gel provides benefits for bioceramics, particularly the chance of acquiring nanostructured pure

This is the accepted manuscript (postprint) of the following article:
E. Salahinejad, R. Vahedifard, *Deposition of nanodiopside coatings on metallic biomaterials to stimulate apatite-forming ability*, Materials and Design 123 (2017) 120–127.
http://dx.doi.org/10.1016/j.matdes.2017.03.047

products with enhanced surface activity [21-24]. Nonetheless, following these synthesis routes, a need for calcination at elevated temperatures around 1100 °C has been reported to obtain single-phase diopside [25, 26], which challenges the preservation of the nanometric structure. On the other hand, after depositing sols containing coprecipitation- and sol-gel-derived nanoparticles or sol-gel solutions, the mentioned firing cycle can result in the damage of metallic substrates, especially stainless steels undergoing intergranular sensitization and corrosion attack [27]. To the best of our knowledge, there is no systematic report about the wet deposition (spin-coating, dip-coating or spray) of precipitation-synthesized diopside on medical-grade stainless steels. In this work, diopside synthesized by a novel coprecipitation process using chloride precursors was successfully deposited on stainless steel 316L by a facile dip-coating method followed by a low-temperature firing process. Then, the *in vitro* bioactivity and biodegradation of the product were evaluated by microscopic and spectroscopic methods.

2. Experimental procedure

Silicon tetrachloride ($SiCl_4$, Merck, Germany, >99%), magnesium chloride ($MgCl_2$, Merck, Germany, >98%), and calcium chloride ($CaCl_2$, Merck, Germany, >98%) precursors were used to synthesize diopside by a coprecipitation method. Also, ethanol (C_2H_5OH, Merck, Germany, >99%) as the solvent and aqueous ammonia solution (NH_4OH, Merck, Germany, 25%) as the precipitating agent were employed. For the coprecipitation synthesis of diopside particles, an equimolar amount of $CaCl_2$ and $MgCl_2$ was dissolved in ethanol. Afterwards, the appropriate content of $SiCl_4$, based on the diopside stoichiometry, was added to the solution while stirring in an ice-water bath. The ammonia solution was then added to

This is the accepted manuscript (postprint) of the following article:
E. Salahinejad, R. Vahedifard, *Deposition of nanodiopside coatings on metallic biomaterials to stimulate apatite-forming ability*, Materials and Design 123 (2017) 120–127.
http://dx.doi.org/10.1016/j.matdes.2017.03.047

the solution to obtain a pH value of about 10, giving white precipitates deposited in the bottom of the beaker under a viscous creamy liquid.

A part of the obtained precipitates, on the one hand, was dried at 120 °C, calcined at 700 °C for 2 h and then analyzed by X-ray diffraction (XRD, Co Kα radiation, scan step size: 0.03°), Fourier transform infrared spectroscopy (FTIR, resolution: 2 cm^{-1}) and transmission electron microscopy (TEM, 200 kV). On the other hand, a part of the rest was several times washed and centrifuged with water to remove coproducts of the precipitation process; and the other part was kept without any processing. To prepare sols from the washed and unwashed precipitates for coating deposition, they were separately dispersed in a proper amount of ethanol and water. Stainless steel 316L substrates were polished by sand papers to # 3000 and then washed by acetone, ethanol and water under ultrasonication. The prepared colloidal suspensions were deposited on the substrates by the dip-coating method at the immersion and withdrawal speeds of 30 mm/s with a dwell time of 30 s. After drying of the coatings at 100 °C for 2 h, they were sintered at 700 °C for 1 and 2 h under an argon atmosphere. The surface-morphology and cross-section of the coatings were studied by field-emission scanning electron microscopy (FESEM). Prior to the SEM observations, the samples were sputter-coated with a thin layer of Au.

To analyze the effect of coating on the *in vitro* bio-performance of the substrate, the optimal coated samples were incubated in the simulated body fluid (SBF) [28] at 37 °C for 1, 3, 7 and 14 days. Concerning apatite-forming ability (bioactivity), the selected soaked samples were studied by FESEM and FTIR. Regarding biodegradation, the concentration of principal ions in the SBF before and after immersion was assessed by inductively coupled plasma spectroscopy (ICP). Also, the pH value of the SBF before and after immersion was measured.

This is the accepted manuscript (postprint) of the following article:
E. Salahinejad, R. Vahedifard, *Deposition of nanodiopside coatings on metallic biomaterials to stimulate apatite-forming ability*, Materials and Design 123 (2017) 120–127.
http://dx.doi.org/10.1016/j.matdes.2017.03.047

3. Results and discussion

Fig. 1(a) presents the XRD spectrum of the powder sample synthesized by the coprecipitation process after calcination at 700 °C for 2 h. According to the analysis of the pattern by the PANalytical X'Pert HighScore software, the powder is merely composed of diopside ($MgCaSi_2O_6$, Ref. code: 00-017-0318) with a monoclinic pyroxene structure without any impurity phase. The crystallite size of diopside is about 50 nm, as calculated by the Scherrer equation for the most intense diffraction peak. The FTIR spectrum of the same sample is also provided in Fig. 1(b). As can be seen, some adsorption modes of O-Ca-O and O-Mg-O appear at about 400 cm^{-1} and in the range of 460 cm^{-1} to 525 cm^{-1}, respectively. Peaks at around 635 and 672 cm^{-1} are related to the O-Si-O bending vibration, while those located at almost 860, 960, 1070 cm^{-1} are assigned to the Si-O stretching modes. The peaks appearing at about 1440 and 1635 cm^{-1} originate from the adsorption of ambient contamination and moisture. It would be worth mentioning that the FTIR assignments are in good agreement with Refs. [29-31]. In conclusion, the FTIR spectroscopy suggests the formation a single-phase diopside structure in the calcined sample, confirming the XRD analysis. The TEM micrograph of the powder also signifies relatively polygonal-shaped particles with an average size of almost 70 nm, as indicated in Fig. 1(c).

The SEM micrographs of the coatings deposited in the different conditions are shown in Fig. 2. According to Fig. 2(a), the coating obtained from the unwashed sol yields an undesirable feature, where it contains a considerable level of inhomogeneity, cracks, discontinuity and uncoated areas. In contrast, from the viewpoint of these mentioned defects, the coatings obtained from the suspensions containing the washed particles have acceptable circumstances, as demonstrated in Figs. 2(b) and 2(c). Hence, it is realized that washing of

This is the accepted manuscript (postprint) of the following article:
E. Salahinejad, R. Vahedifard, *Deposition of nanodiopside coatings on metallic biomaterials to stimulate apatite-forming ability*, Materials and Design 123 (2017) 120–127.
http://dx.doi.org/10.1016/j.matdes.2017.03.047

the precipitates improves the film's quality, via eliminating the coprecipitation coproduct (NH_4Cl, so that NH_4^+ and Cl^- originate from the precipitating agent and precursors, respectively). It is due to the fact that, on the one hand, chloride ions existing in the sol reduce the stability and wettability of the sol, thereby deteriorating the quality of the obtained coating [32, 33]. The considerable stability of the sol achieved from the washed precipitates, followed by the dip-coating deposition and the leave of the liquid phase, refers to the particulate sol-gel process. On the other hand, in the presence of NH_4Cl dissolved in the sol, the dried coating contains a significant amount of this solid which sublimes during heating in the sintering process with a high level of shrinkage, which encourages the development of cracks in the coating. Note that considering the stoichiometric content of chloride in the precursors, it can be estimated that the volume ratio of NH_4Cl to the synthesized nanoparticles is almost 6.5 after the coprecipitation synthesis route.

In addition, as shown in Figs. 2(b), even at this relatively low magnification, the coating obtained from the washed sol after sintering at 700 °C for 1 h represents a particulate nature without a considerable cohesion of the nanoparticles. In contrast, based on Figs. 2(c), an apparently integrated coating with a good cohesion is developed for the sintering period of 2 h, as is evident in the same magnification. Thus, it is realized that the increase of the sintering period from 1 h to 2 h effectively improves the film's cohesion, despite the fact that the particulate nature of the latter coating is apparent in the higher magnification micrograph (Fig. 2(d)). According to this micrograph, the coating is mainly composed of polygonal diopside nanoparticles of 70 nm in size, confirming the TEM observation (Fig. 1(c)). Anyway, the coatings obtained from the washed precipitates after sintering at 700 °C for 2 h are regarded as the optimal coating and only characterized below.

This is the accepted manuscript (postprint) of the following article:
E. Salahinejad, R. Vahedifard, *Deposition of nanodiopside coatings on metallic biomaterials to stimulate apatite-forming ability*, Materials and Design 123 (2017) 120–127.
http://dx.doi.org/10.1016/j.matdes.2017.03.047

Fig. 3 shows the cross-sectional SEM micrograph of the optimal coating in two magnifications. The low-magnification micrograph (Fig. 3(a)) exhibits the deposited coating with a relatively uniform thickness of about 2 μm. In addition, the higher-magnification micrograph (Fig. 3(b)) suggests the two following points. First, an acceptable adhesion of the coating and substrate is achieved due to sintering, as explained by an oxygen-shared mechanism [14, 34]. Second, the coating contains a number of open and closed nanopores, which verifies its particulate nature and can albeit be advantageous to bioactivity via providing a higher surface area [35-37].

The SEM micrographs of the coated samples after 3 and 7 days of soaking in the SBF are shown in Fig. 4. A comparison between the surfaces before (Fig. 2) and after (Fig. 4) immersion points out the deposition of new precipitates on the surface as a result of incubation, as characterized below to be a kind of apatite (calcium phosphate). This is in contrast to the uncoated stainless steel 316L which presents no typical apatite-mineralization ability. That is, the deposition of nanodiopside on stainless steel 316L considerably encourages biomineralization.

According to Figs. 4(a), 4(b) and 4(c), the coated surface after 3 days of immersion in the SBF shows a complete coverage of the apatite-like precipitates. In the higher-magnification micrographs, it is evident that the coating's surface is uniformly covered by a layer of non-dense intersecting irregularly-oriented plates with the averages of 20 and 180 nm in the smallest and largest dimensions, respectively, and an average of 150 nm in spacing. Thus, it can be inferred that the early stages of the apatite precipitation on the nanodiopside coating are uniform and integrated. In the case of sintering at 1100 °C giving micron-sized diopside, nevertheless, the apatite layers deposited after immersion in the SBF present unlike appearances [25, 26]. The uniform feature of the precipitates at the early stages of the current

This is the accepted manuscript (postprint) of the following article:
E. Salahinejad, R. Vahedifard, *Deposition of nanodiopside coatings on metallic biomaterials to stimulate apatite-forming ability*, Materials and Design 123 (2017) 120–127.
http://dx.doi.org/10.1016/j.matdes.2017.03.047

work is attributed to the nanometric size of diopside providing a considerably high level of interfaces as the nucleation sites of apatite (Fig. 2(d)).

The comparison of the SEM micrographs of the samples after 3 and 7 days of soaking in the SBF (Fig. 4) reflects some notes. By increasing the soaking time from 3 days to 7 days, on the one hand, the dimensions and packing of the uniform plates is enhanced due to the evolution of apatite precipitation. On the other hand, a number of new precipitates with a rose-like morphology, which non-uniformly cover the surface, are formed on the sample's surface. As seen in Fig. 4(d), the mean diameter and spacing of the flowers are about 1.2 and 2.5 μm, respectively. According to the high-magnification micrographs showed in Figs. 4(e) and 4(f), the average thickness of each leaf of the roses is almost 35 nm. It is noticeable that the leaf-like deposits are precipitated on a relatively dense nanodiopside substrate, while the flowers are grown on a non-dense leaf-like apatite layer previously-precipitated *in vitro*. It is accordingly believed that the different morphologies of the deposits at the different stages of incubation in the SBF can be due to their different direct substrates (as noted above) and/or the different ionic compositions of their real-time SBF (as determined below by the ICP method). Anyway, the observation of these morphologies of apatite at these incubation periods is indicative of substantial bioactivity, as a similar appearance of apatite precipitated *in vitro* on the surface of apatite- and wollastonite-containing glass-ceramics (which are known to be considerably bioactive) has been reported [38].

Fig. 5 demonstrates the FTIR spectra of the samples after incubation in the SBF for 3 and 7 days. As depicted in Fig. 5(a), the bending (at about 480 and 500 cm^{-1}) and stretching (at around 970 and 1080 cm^{-1}) vibration modes of phosphate appear in the FTIR pattern of the sample after 3 days of immersion. In the same pattern, a low-intensity adsorption signal of carbonate is detected at almost 875 cm^{-1}. However, the hydroxyl group is straightforwardly

This is the accepted manuscript (postprint) of the following article:
E. Salahinejad, R. Vahedifard, *Deposition of nanodiopside coatings on metallic biomaterials to stimulate apatite-forming ability*, Materials and Design 123 (2017) 120–127.
http://dx.doi.org/10.1016/j.matdes.2017.03.047

detected from the peaks of around 1640 and 3425 cm^{-1}. Regarding the sample immersed in the SBF for 7 days (Fig. 5(b)), as well as the above-mentioned vibrations, the higher levels of carbonate in the sample is identified from the additional adsorption bands of around 1420 and 1460 cm^{-1}. In addition, the intensity of the hydroxyl vibrations is reduced in comparison to the sample soaked in the SBF for 3 days. This means that a higher level of carbonate substitutes for hydroxyl in the apatite deposits by increasing the incubation time from 3 days to 7 days. Note that the FTIR assignments are also in agreement with Refs. [39, 40]. Considering the above morphological assessments (Fig. 4) in parallel with the FTIR analysis (Fig. 5), it is inferred that the leaf-like precipitates formed until the 3rd day are hydroxycarbonated apatite (HCA) with a lower level of carbonate in comparison to the rose-like HCA deposits detected on the 7th day of incubation.

To study biodegradation and thereby to recognize the bioactivity mechanism of the coating, the concentrations of Ca, Mg, Si and P ions in the SBF before and after incubating the samples for the different periods were measured by the ICP analysis (Fig. 6). As can be observed, the ionic concentration of Ca in the SBF is progressively increased from about 100 ppm to 142 ppm for 0 to 14 days of immersion, respectively. This suggests the dissolution of Ca from the diopside coating into the SBF, which is vital for an effective deposition of apatite on the sample's surface via providing a supersaturated solution. A similar increasing trend, but with a lower slope, is also observed for Mg ions. Although the Mg species does not directly participate in the apatite structure, its presence in the medium encourages the deposition of amorphous apatite, but inhibits apatite crystallization [41, 42]. The concentration of the Si species also shows a sharp increase for the first day, then a slow enhancement to the third day, and finally a relatively constant value to 14 days of immersion. It would be worth mentioning that the presence of Si in the SBF independently is indicative

This is the accepted manuscript (postprint) of the following article:
E. Salahinejad, R. Vahedifard, *Deposition of nanodiopside coatings on metallic biomaterials to stimulate apatite-forming ability*, Materials and Design 123 (2017) 120–127.
http://dx.doi.org/10.1016/j.matdes.2017.03.047

of the degradation of the immersed sample, since the SBF before immersion is Si-free. More importantly, the concentration of P experiences a progressive decrease during the tested period due to the deposition of a P-containing phase i.e. apatite, as characterized above by the SEM and FTIR analyses.

The study of variations in the pH value of the SBF with immersion time is another approach to explaining the variations detected in the concentration of SBF and thereby biomineralization. Before soaking the samples, the SBF has the standard pH value of 7.4. As showed in Fig. 7, pH increases to almost 8 to the 7th day of immersion. Because in accordance with the ICP analysis, nanodiopside releases Mg^{2+} and Ca^{2+} into the SBF; subsequently, the resultant vacancies absorbs a number of H^{+} ions of the SBF, increasing pH. The next decrease in pH to 14 days of incubation can be explained by the development of HA and HCA precipitations which consume hydroxyl dissolved in the SBF.

Eventually, considering the variations in the ionic concentrations and pH of the SBF with soaking time, a typical ion-exchange reaction is recognized as the mechanism for *in vitro* apatite-mineralization of diopside as a result of immersion in the SBF. The dissolution of Ca and Mg ions from nanodiopside, as realized from the ICP studies (Fig. 6), provides a surface layer enriched with the silanol (Si–OH) groups. It is believed that these surface silanol groups have a critical contribution to apatite deposition, via adsorbing Ca cations from the supersaturated SBF. The accumulation of these cations on the surface encourages the subsequent adsorption of phosphate, carbonate and hydroxyl anions of the SBF. The deposition of these ions on the surface gives rise to the formation of the related apatite phases, as characterized by the FTIR analysis (Fig. 5). It is noteworthy that a similar mechanism is responsible for the appropriate apatite-forming ability of bioactive glasses and

This is the accepted manuscript (postprint) of the following article:
E. Salahinejad, R. Vahedifard, *Deposition of nanodiopside coatings on metallic biomaterials to stimulate apatite-forming ability*, Materials and Design 123 (2017) 120–127.
http://dx.doi.org/10.1016/j.matdes.2017.03.047

glass-ceramics [43-46]; alternatively, moderately bioactive ceramics like titanates predominantly represent a hydrophilicity-based mechanism for biomineralization [47, 48].

4. Conclusions

In this work, coprecipitation-derived diopside coatings on stainless steel 316L with a uniform and crack-free feature and a mean thickness of almost 2 μm were developed by dip-coating and sintering at 700 °C for 2 h. The immersion of the coated samples in the SBF induced a suitable apatite-forming ability to the substrate, in the form of hydroxycarbonate apatite. In this regard, the formed apatite layer presented an integrated leaf-like feature at the early stages and a next non-uniform flower-like appearance, with a tendency to the increase of carbonate with the incubation time. The deposited diopside coating showed a degradable behavior in the SBF, accompanied by a reduction in the concentration of P in the SBF with incubation time. It was eventually pointed out that the aforementioned ion-exchange reaction controls the *in vitro* apatite-mineralization of the nanodiopside coating.

References

[1] F. Mahyudin, H. Hermawan, Biomaterials and Medical Devices: A Perspective from an Emerging Country, Springer, 2016.
[2] M. Niinomi, T. Narushima, M. Nakai, Advances in Metallic Biomaterials: Tissues, Materials and Biological Reactions, Springer, 2015.
[3] M. Niinomi, Recent metallic materials for biomedical applications, Metallurgical and materials transactions A, 33 (2002) 477-486.
[4] E. Salahinejad, M.J. Hadianfard, D.D. Macdonald, S. Sharifi-Asl, M. Mozafari, K.J. Walker, A.T. Rad, S.V. Madihally, L. Tayebi, In vitro electrochemical corrosion and cell viability studies on nickel-free stainless steel orthopedic implants, PloS one, 8 (2013) e61633.
[5] M.B. Nasab, M.R. Hassan, B.B. Sahari, Metallic biomaterials of knee and hip-A review, Trends Biomater. Artif. Organs, 24 (2010) 69-82.
[6] M. Navarro, A. Michiardi, O. Castano, J. Planell, Biomaterials in orthopaedics, Journal of the Royal Society Interface, 5 (2008) 1137-1158.

[7] A.P. Tomsia, E. Saiz, J. Song, C.R. Bertozzi, Biomimetic bonelike composites and novel bioactive glass coatings, Advanced Engineering Materials, 7 (2005) 999-1004.
[8] K. Pardun, L. Treccani, E. Volkmann, G. Li Destri, G. Marletta, P. Streckbein, C. Heiss, K. Rezwan, Characterization of Wet Powder-Sprayed Zirconia/Calcium Phosphate Coating for Dental Implants, Clinical implant dentistry and related research, 17 (2015) 186-198.
[9] F. Baino, J. Minguella, N. Kirk, M.A. Montealegre, C. Fiaschi, F. Korkusuz, G. Orlygsson, V.-B. Chiara, Novel full-ceramic monoblock acetabular cup with a bioactive trabecular coating: design, fabrication and characterization, Ceramics International, 42 (2016) 6833-6845.
[10] F. Baino, C. Vitale-Brovarone, Feasibility of glass–ceramic coatings on alumina prosthetic implants by airbrush spraying method, Ceramics International, 41 (2015) 2150-2159.
[11] E. Salahinejad, M. Hadianfard, D. Vashaee, L. Tayebi, Influence of annealing temperature on the structural and anti-corrosion characteristics of sol–gel derived, spin-coated thin films, Ceramics International, 40 (2014) 2885-2890.
[12] M. Mozafari, E. Salahinejad, S. Sharifi-Asl, D. Macdonald, D. Vashaee, L. Tayebi, Innovative surface modification of orthopaedic implants with positive effects on wettability and in vitro anti-corrosion performance, Surface Engineering, 30 (2014) 688-692.
[13] E. Salahinejad, M. Hadianfard, D. Macdonald, M. Mozafari, K. Walker, A.T. Rad, S. Madihally, D. Vashaee, L. Tayebi, Surface modification of stainless steel orthopedic implants by sol–gel ZrTiO4 and ZrTiO4–PMMA coatings, Journal of biomedical nanotechnology, 9 (2013) 1327-1335.
[14] E. Salahinejad, M. Hadianfard, D. Macdonald, M. Mozafari, D. Vashaee, L. Tayebi, A new double-layer sol–gel coating to improve the corrosion resistance of a medical-grade stainless steel in a simulated body fluid, Materials Letters, 97 (2013) 162-165.
[15] M. Mozafari, E. Salahinejad, V. Shabafrooz, M. Yazdimamaghani, D. Vashaee, L. Tayebi, Multilayer bioactive glass/zirconium titanate thin films in bone tissue engineering and regenerative dentistry, Int J Nanomedicine, 8 (2013) 1665-1672.
[16] E. Salahinejad, M. Hadianfard, D. Macdonald, M. Mozafari, D. Vashaee, L. Tayebi, Multilayer zirconium titanate thin films prepared by a sol–gel deposition method, Ceramics International, 39 (2013) 1271-1276.
[17] M. Mirak, M. ALizadeh, E. Salahinejad, R. Amini, Zn–HA–TiO2 nanocomposite coatings electrodeposited on a NiTi shape memory alloy, Surface and Interface Analysis, 47 (2015) 176-183.
[18] M. Diba, O.-M. Goudouri, F. Tapia, A.R. Boccaccini, Magnesium-containing bioactive polycrystalline silicate-based ceramics and glass-ceramics for biomedical applications, Current Opinion in Solid State and Materials Science, 18 (2014) 147-167.
[19] M. Diba, F. Tapia, A.R. Boccaccini, L.A. Strobel, Magnesium-containing bioactive glasses for biomedical applications, International Journal of Applied Glass Science, 3 (2012) 221-253.
[20] T. Nonami, S. Tsutsumi, Study of diopside ceramics for biomaterials, Journal of Materials Science: Materials in Medicine, 10 (1999) 475-479.
[21] S. Rastegari, O.S.M. Kani, E. Salahinejad, S. Fadavi, N. Eftekhari, A. Nozariasbmarz, L. Tayebi, D. Vashaee, Non-hydrolytic sol-gel processing of chloride precursors loaded at forsterite stoichiometry, Journal of Alloys and Compounds, 688 (2016) 235-241.
[22] E. Salahinejad, M. Hadianfard, D. Vashaee, L. Tayebi, Effect of precursor solution pH on the structural and crystallization characteristics of sol–gel derived nanoparticles, Journal of Alloys and Compounds, 589 (2014) 182-184.
[23] P. Rouhani, E. Salahinejad, R. Kaul, D. Vashaee, L. Tayebi, Nanostructured zirconium titanate fibers prepared by particulate sol–gel and cellulose templating techniques, Journal of Alloys and Compounds, 568 (2013) 102-105.

[24] E. Salahinejad, M. Hadianfard, D. Macdonald, I. Karimi, D. Vashaee, L. Tayebi, Aqueous sol–gel synthesis of zirconium titanate (ZrTiO 4) nanoparticles using chloride precursors, Ceramics International, 38 (2012) 6145-6149.
[25] N.Y. Iwata, G.-H. Lee, Y. Tokuoka, N. Kawashima, Sintering behavior and apatite formation of diopside prepared by coprecipitation process, Colloids and Surfaces B: Biointerfaces, 34 (2004) 239-245.
[26] N.Y. Iwata, G.-H. Lee, S. Tsunakawa, Y. Tokuoka, N. Kawashima, Preparation of diopside with apatite-forming ability by sol–gel process using metal alkoxide and metal salts, Colloids and Surfaces B: Biointerfaces, 33 (2004) 1-6.
[27] C. Tedmon, D. Vermilyea, J. Rosolowski, Intergranular corrosion of austenitic stainless steel, journal of the Electrochemical Society, 118 (1971) 192-202.
[28] T. Kokubo, H. Takadama, How useful is SBF in predicting in vivo bone bioactivity?, Biomaterials, 27 (2006) 2907-2915.
[29] K. Omori, Analysis of infrared absorption spectrum of diopside, American Mineralogist, 56 (1971) 1607-&.
[30] R. Choudhary, J. Vecstaudza, G. Krishnamurithy, H.R.B. Raghavendran, M.R. Murali, T. Kamarul, S. Swamiappan, J. Locs, In-vitro bioactivity, biocompatibility and dissolution studies of diopside prepared from biowaste by using sol–gel combustion method, Materials Science and Engineering: C, 68 (2016) 89-100.
[31] M.J. Baghjeghaz, E. Salahinejad, Enhanced sinterability and in vitro bioactivity of diopside through fluoride doping, Ceramics International, (2016).
[32] A.C. Geiculescu, H.G. Spencer, Thermal decomposition and crystallization of aqueous sol-gel derived zirconium acetate gels: Effects of the precursor solution pH, Journal of sol-gel science and technology, 16 (1999) 243-256.
[33] E. Salahinejad, M. Hadianfard, D. Macdonald, M. Mozafari, D. Vashaee, L. Tayebi, Zirconium titanate thin film prepared by an aqueous particulate sol–gel spin coating process using carboxymethyl cellulose as dispersant, Materials Letters, 88 (2012) 5-8.
[34] S. Dallaire, B. Arsenault, A. Desantis, Investigation of selected plasma-sprayed coatings for bonding glass to metal in hermetic seal applications, Surface and Coatings Technology, 53 (1992) 129-135.
[35] L. Zhang, Z. He, Y. Zhang, Y. Jiang, R. Zhou, Enhanced in vitro bioactivity of porous NiTi–HA composites with interconnected pore characteristics prepared by spark plasma sintering, Materials & Design, 101 (2016) 170-180.
[36] R. Ghosh, R. Sarkar, S. Paul, Development of machinable hydroxyapatite-lanthanum phosphate composite for biomedical applications, Materials & Design, 106 (2016) 161-169.
[37] H. Ghomi, R. Emadi, S.H. Javanmard, Fabrication and characterization of nanostructure diopside scaffolds using the space holder method: Effect of different space holders and compaction pressures, Materials & Design, 91 (2016) 193-200.
[38] J.A. Juhasz, S.M. Best, A.D. Auffret, W. Bonfield, Biological control of apatite growth in simulated body fluid and human blood serum, Journal of Materials Science: Materials in Medicine, 19 (2008) 1823-1829.
[39] I. Rehman, W. Bonfield, Characterization of hydroxyapatite and carbonated apatite by photo acoustic FTIR spectroscopy, Journal of Materials Science: Materials in Medicine, 8 (1997) 1-4.
[40] A. Ślósarczyk, Z. Paszkiewicz, C. Paluszkiewicz, FTIR and XRD evaluation of carbonated hydroxyapatite powders synthesized by wet methods, Journal of Molecular Structure, 744 (2005) 657-661.
[41] C.S. Martens, R.C. Harriss, Inhibition of apatite precipitation in the marine environment by magnesium ions, Geochimica et Cosmochimica Acta, 34 (1970) 621-625.

This is the accepted manuscript (postprint) of the following article:
E. Salahinejad, R. Vahedifard, *Deposition of nanodiopside coatings on metallic biomaterials to stimulate apatite-forming ability*, Materials and Design 123 (2017) 120–127.
http://dx.doi.org/10.1016/j.matdes.2017.03.047

[42] Y. Cai, S. Zhang, X. Zeng, Y. Wang, M. Qian, W. Weng, Improvement of bioactivity with magnesium and fluorine ions incorporated hydroxyapatite coatings via sol–gel deposition on Ti6Al4V alloys, Thin Solid Films, 517 (2009) 5347-5351.
[43] A. Hoppe, N.S. Güldal, A.R. Boccaccini, A review of the biological response to ionic dissolution products from bioactive glasses and glass-ceramics, Biomaterials, 32 (2011) 2757-2774.
[44] J. Davis, Overview of biomaterials and their use in medical devices, Handbook of materials for medical devices. Illustrated edition, Ohio: ASM International, (2003) 1-11.
[45] O. Peitl, E.D. Zanotto, L.L. Hench, Highly bioactive P 2 O 5–Na 2 O–CaO–SiO 2 glass-ceramics, Journal of Non-Crystalline Solids, 292 (2001) 115-126.
[46] P. Saravanapavan, J.R. Jones, R.S. Pryce, L.L. Hench, Bioactivity of gel–glass powders in the CaO-SiO2 system: A comparison with ternary (CaO-P2P5-SiO2) and quaternary glasses (SiO2-CaO-P2O5-Na2O), Journal of Biomedical Materials Research Part A, 66 (2003) 110-119.
[47] K.B. Devi, K. Singh, N. Rajendran, Sol–gel synthesis and characterisation of nanoporous zirconium titanate coated on 316L SS for biomedical applications, Journal of sol-gel science and technology, 59 (2011) 513-520.
[48] T. Kokubo, Design of bioactive bone substitutes based on biomineralization process, Materials Science and Engineering: C, 25 (2005) 97-104.

This is the accepted manuscript (postprint) of the following article:
E. Salahinejad, R. Vahedifard, *Deposition of nanodiopside coatings on metallic biomaterials to stimulate apatite-forming ability*, Materials and Design 123 (2017) 120–127.
http://dx.doi.org/10.1016/j.matdes.2017.03.047

Figures

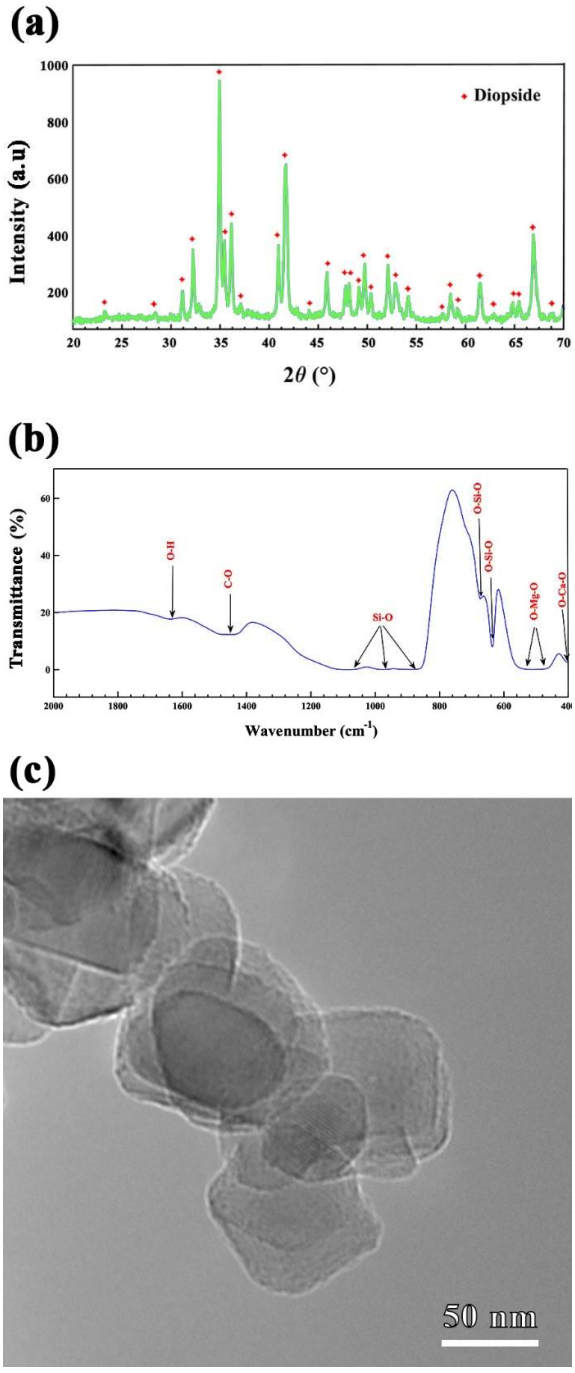

Fig. 1. XRD pattern (a), FTIR spectrum (b), and TEM micrograph (c) of the powder sample calcined at 700 °C for 2 h (non-labeled peaks belong to diopside).

This is the accepted manuscript (postprint) of the following article:
E. Salahinejad, R. Vahedifard, *Deposition of nanodiopside coatings on metallic biomaterials to stimulate apatite-forming ability*, Materials and Design 123 (2017) 120–127.
http://dx.doi.org/10.1016/j.matdes.2017.03.047

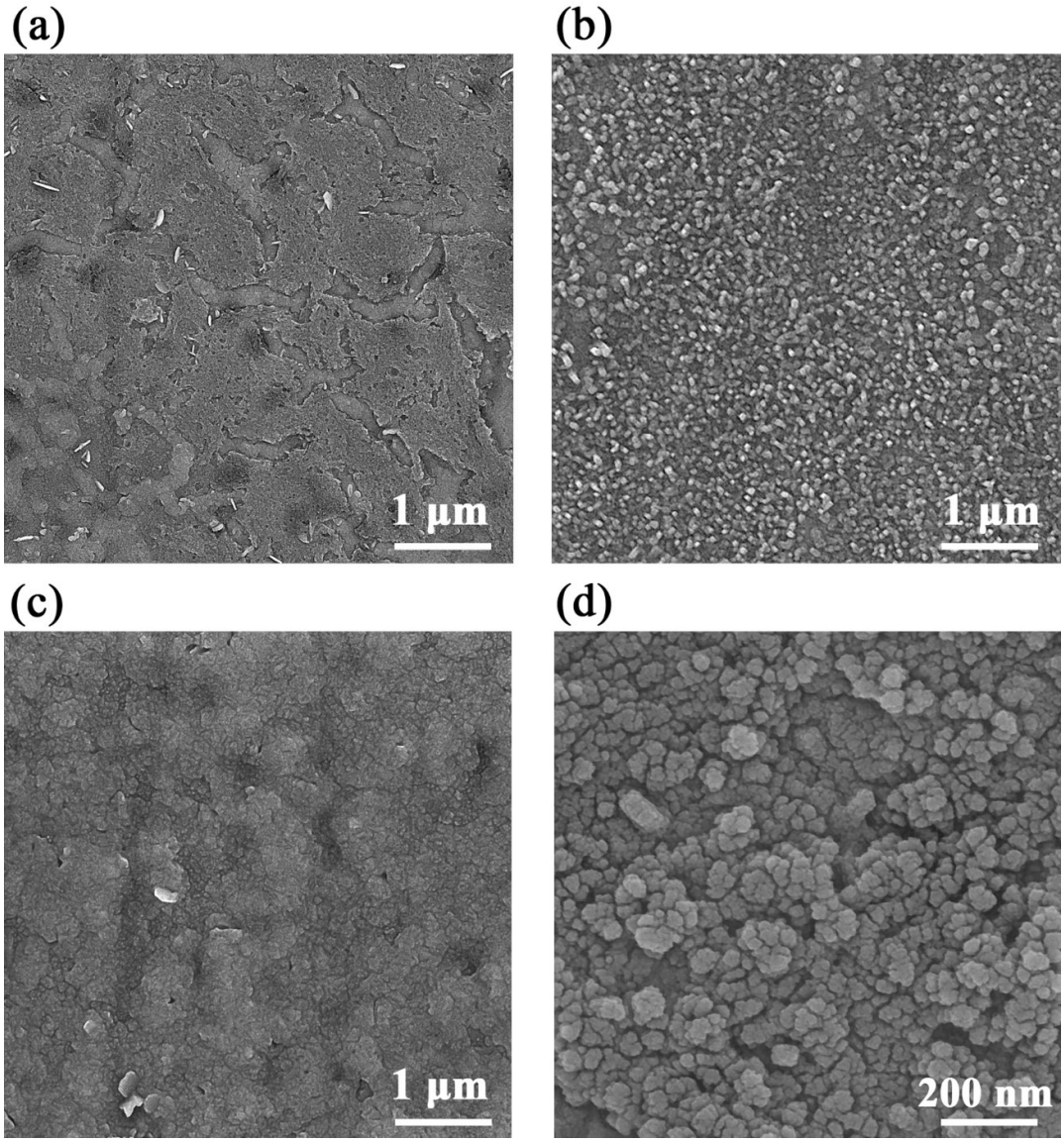

Fig. 2. Top-view SEM micrographs of the coatings prepared: without washing of the synthesized precipitates, after sintering at 700 °C (a), after washing and sintering at 700 °C for 1 h (b), and after washing and sintering at 700 °C for 2 h in two magnifications (c, d).

This is the accepted manuscript (postprint) of the following article:
E. Salahinejad, R. Vahedifard, *Deposition of nanodiopside coatings on metallic biomaterials to stimulate apatite-forming ability*, Materials and Design 123 (2017) 120–127.
http://dx.doi.org/10.1016/j.matdes.2017.03.047

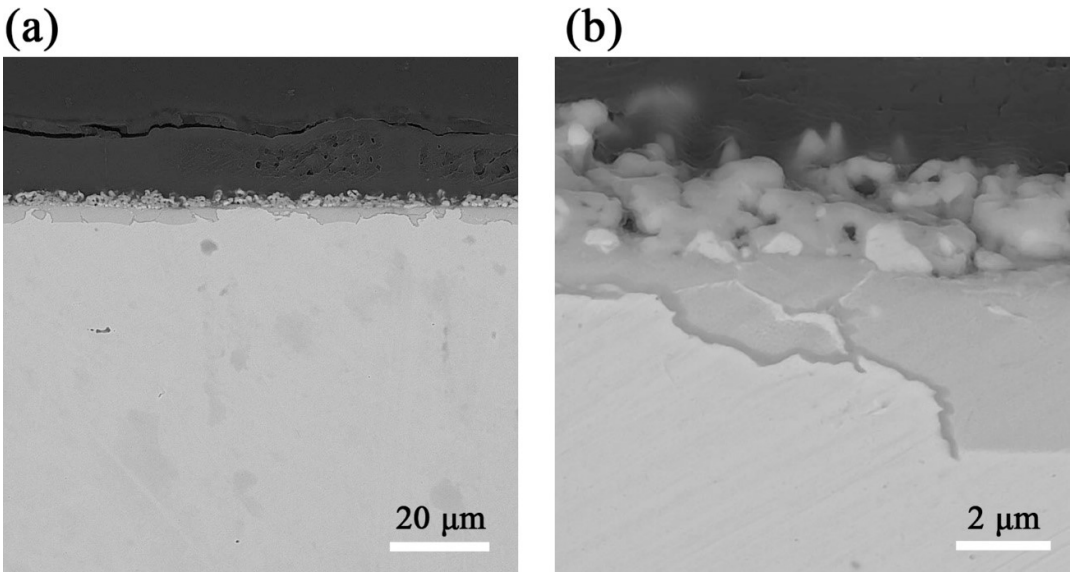

Fig. 3. Low-magnification (a) and high-magnification (b) cross-sectional SEM micrographs of the coating sample after washing and sintering at 700 °C for 2 h.

This is the accepted manuscript (postprint) of the following article:
E. Salahinejad, R. Vahedifard, *Deposition of nanodiopside coatings on metallic biomaterials to stimulate apatite-forming ability*, Materials and Design 123 (2017) 120–127.
http://dx.doi.org/10.1016/j.matdes.2017.03.047

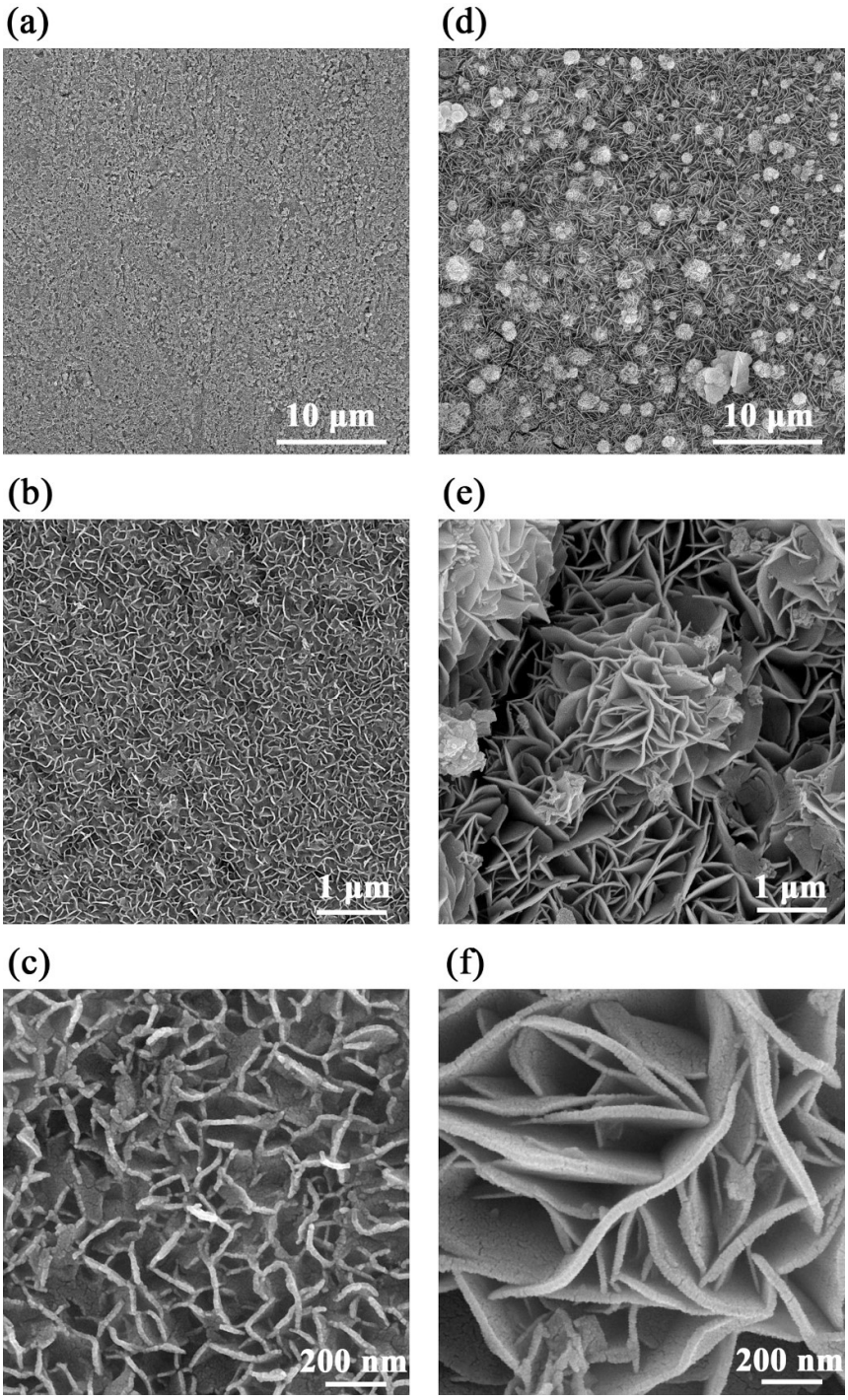

Fig. 4. SEM micrographs of the samples after soaking in the SBF for 3 (a, b, c) and 7 days (d, e, f) in three magnifications.

This is the accepted manuscript (postprint) of the following article:
E. Salahinejad, R. Vahedifard, *Deposition of nanodiopside coatings on metallic biomaterials to stimulate apatite-forming ability*, Materials and Design 123 (2017) 120–127.
http://dx.doi.org/10.1016/j.matdes.2017.03.047

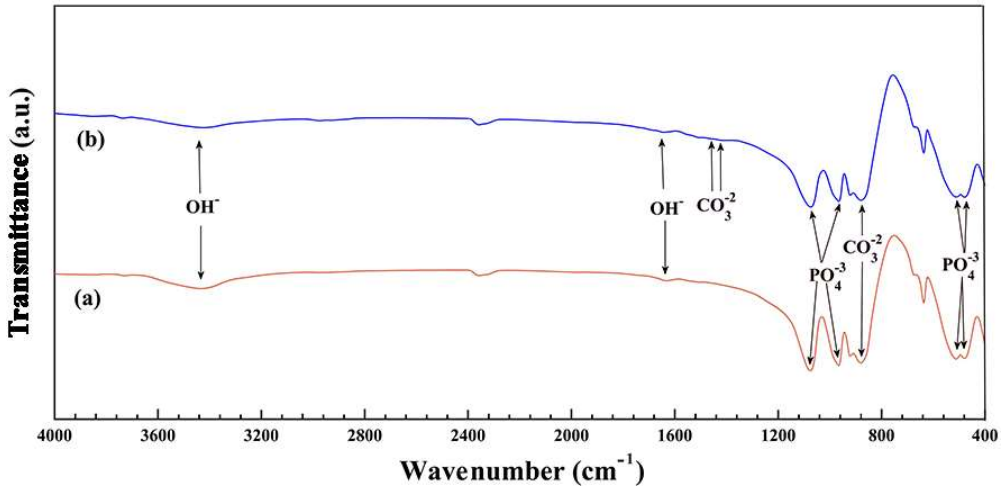

Fig. 5. FTIR spectra of the powder samples after 3 (a) and 7 (b) days of immersion in the SBF.

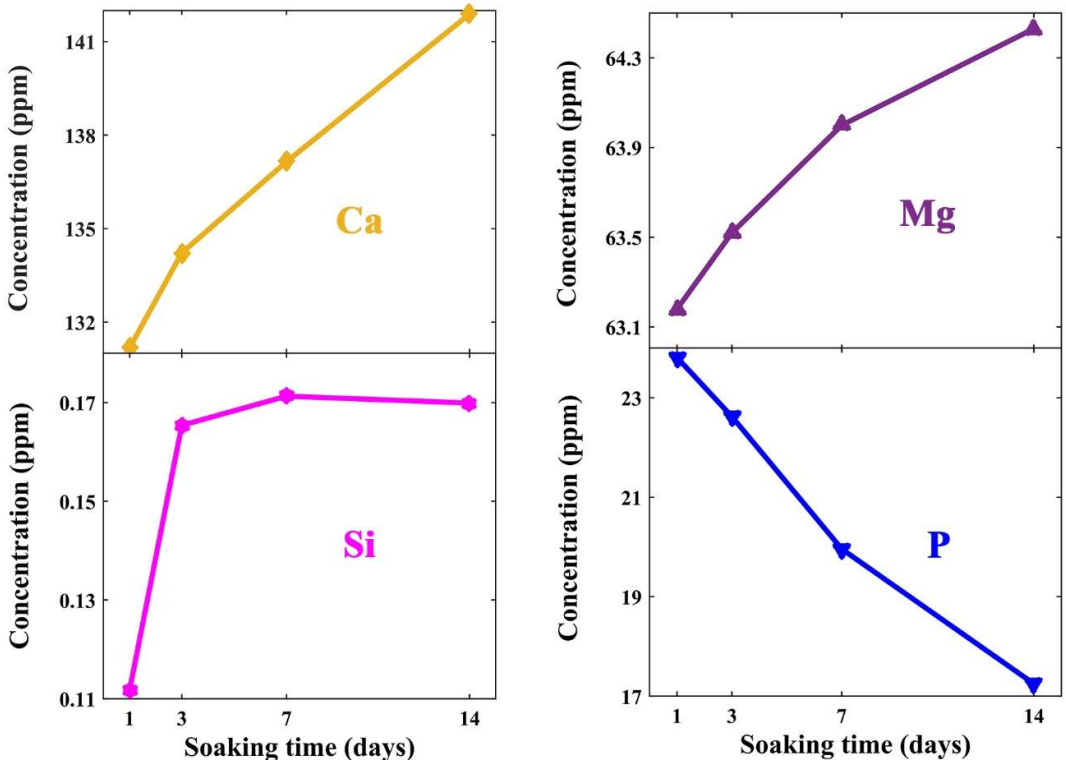

Fig. 6. ICP results on the SBF after incubation of the coated samples for the various durations.

This is the accepted manuscript (postprint) of the following article:
E. Salahinejad, R. Vahedifard, *Deposition of nanodiopside coatings on metallic biomaterials to stimulate apatite-forming ability*, Materials and Design 123 (2017) 120–127.
http://dx.doi.org/10.1016/j.matdes.2017.03.047

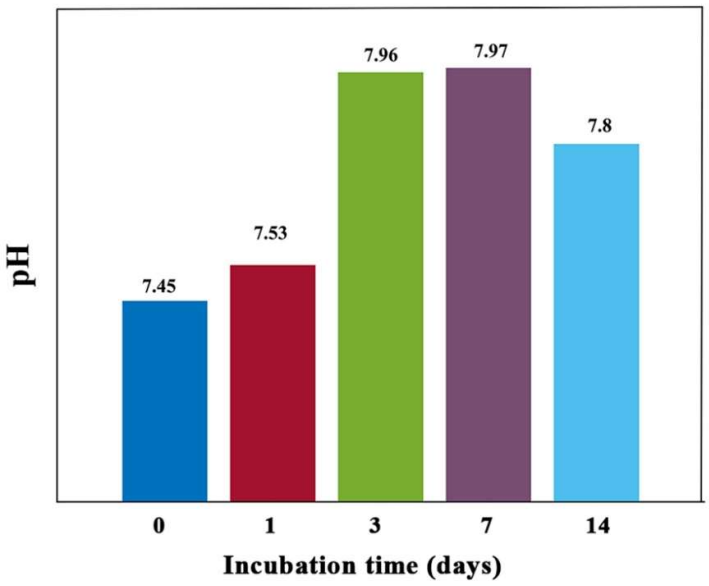

Fig. 7. pH value of the SBF after incubation of the coated samples for the various durations.